ACS OMEGA

http://pubs.acs.org/journal/acsodf

Article

Electromagnetic Trihybrid Ellis Nanofluid Flow Influenced with a Magnetic Dipole and Chemical Reaction Across a Vertical Surface

Muhammad Rooman, Anwar Saeed, Zahir Shah,* Ahmed Alshehri, Saeed Islam, Poom Kumam,* and Panawan Suttiarporn

Cite This: *ACS Omega* 2022, 7, 36611−36622

Read Online

ACCESS | Metrics & More | Article Recommendations

ABSTRACT: The purpose of this study is to evaluate the augmentation of thermal energy transfer in trihybrid Ellis nanofluid flow in the occurrence of magnetic dipole passes over a vertical surface. The ternary hybrid nanofluid is prepared by the dispersion of ternary nanoparticles (Al_2O_3, SiO_2, and TiO_2) in the Carreau Yasuda fluid. The velocity and heat transportation has been examined in the existence of the Darcy Forchhemier influence and heat source/sink. The phenomena of fluid flow have been mathematically designed for energy and fluid velocity in the form of a nonlinear partial differential equation (PDE)-based system. The system of PDEs is further refined to the set of ordinary differential equations via suitable similarity substitutions. The acquired dimensionless equations are numerically solved with the help of the HAM. It has been noticed that the energy contour is enhanced versus the variation of viscous dissipation and heat generation. A significant contribution of a magnetic dipole is observed to elevate the production of the thermal energy field, and an opposite trend is noticed versus the flow profile. The accumulation of Al_2O_3, SiO_2, and TiO_2 nanomaterials in the base fluid "engine oil" improves the velocity and energy profiles.

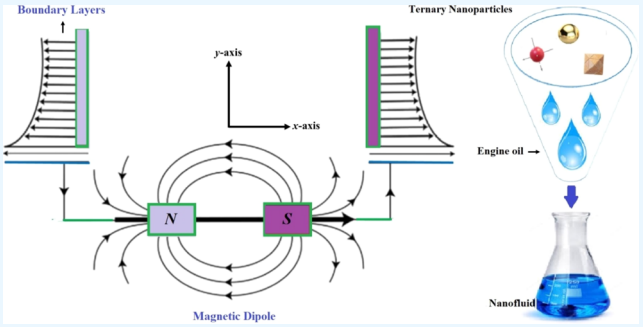

1. INTRODUCTION

The analysis of nanofluid flow over a vertical surface with heat transaction properties has received great interest due to its major engagement in industrial requirements and recent developments.[1] Hosseinzadeh et al.[2] scrutinized the micropolar MHD (magneto-hydrodynamics) fluid flow moving across an upright plate with three distinct base fluids: ethylene glycol, ethylene glycol/water, and water. The thermal gradient of lamina-shaped nanoparticles (nps) in water-based fluids is 38.09 percent advanced tendency than common nps, according to the findings. Reddy et al.[3] designated an arithmetical analysis of an entropy generation on unsteady ferrofluid flow and mixed convection over an infinite vertical surface. Fluid flow across a vertical surface has a variety of uses in geothermal technology, petroleum extraction, oil drilling, and barrier properties, according to the study. Haq et al.[4] explored the energy conduction of an unsteady nanoliquid flow with the MHD effect across an indefinite vertical sheet. Kumar et al.[5] evaluated the effects of Dufour and thermal radiation on an MHD boundary layer flow across a permeable media. Algehyne et al.[6] reported the bioconvection generated by the MHD flow of a hybrid ferrofluid consisting of nanomaterials through a vertical substrate. The influence of the porosity component and buoyancy ratio on the velocity trajectory has been noticed. The energy transformation characteristic improves dramatically as Eckert number and thermal absorption/generation levels rise. Dadheech et al.[7] demonstrated the development of entropy in nanofluid flow over permeable and vertical plates. Kodi et al.[8] demonstrated the nanofluid flow with energy transport properties, influenced by chemical reactivity. Shah et al.[9] evaluated the thermophoresis effect, concentration diffusivity, and variable viscosity over a vertical plate. Shah et al.[10] examined the effect of the AB noninteger derivative with trihybrid nano particulates suspension across a vertical surface. Hussain et al.[11] numerically reported the effectiveness of thermal features over a nonuniform vertical surface with heat generation through Carreau fluid. Some related recent studies have been reported.[12−17]

Fluid flow can be classified as Newtonian or non-Newtonian. Various natural fluids, such as air and water, have been considered to be Newtonian fluids for research purposes. When fluid flow defied Newton's model, there was a strong demand for a new concept. Numerous theories were put to the

Received: July 21, 2022
Accepted: September 20, 2022
Published: October 5, 2022

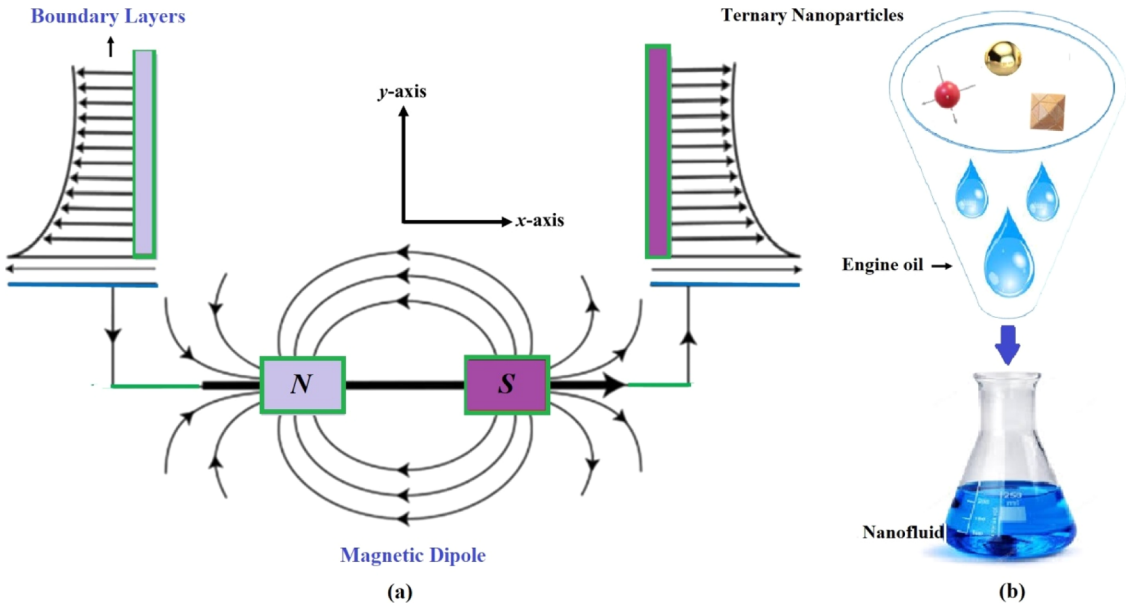

Figure 1. Physical sketch of the proposed model.

test in order to completely categorize the nature of these non-Newtonian viscoelastic substances, but the issue remained. The important feature of Ellis fluid is that it can indicate viscous fluid behavior at small shear stresses and Ostwald de Waele fluid behavior at elevated shear stresses. The Ellis fluid displays shear thinning and thickening characteristics at low, moderate, and high stress rates. Kheyfets and Kieweg[18] demonstrated three-dimensional simulations of the constant-volume, gravity-driven unrestricted surface flow of an Ellis fluid by using thin film lubrication estimation. Javed et al.[19] examined the calendaring of the Ellis fluid using the lubrication approximation theory. Celli et al.[20] evaluated the onset of convective instability within a horizontal porous layer coated with a non-Newtonian fluid. They assumed fluid is shear−thinning, and the Ellis model defines its apparent viscosity. Sajid et al.[21] investigated the flow in the renal tubule using Ellis fluid model. Rooman et al.[22] investigated the entropy formation and its influences on Ellis fluid flow. They considered a porous horizontal stretching cylinder with an MHD effect. Shah et al.[23] investigated, at a low Reynolds number, the mathematical model associated with bacterial gliding mechanism using the Ellis fluid model.

In the modern era, hybrid nanofluid has been heavily used to boost heat conductivity. Renewable energy, microelectronics, emollients, automotive industry, electronic cooling, generators, nuclear coolant system, ships, and biomedicine development are all the usages of hybrid nanofluids.[24−27] Yahya et al.[28] investigated a hybrid nanofluid flow in engine oil including zinc oxide (ZnO) and molybdenum disulfide (MoS_2) nps across an elongating sheet. Rehman et al.[29] proposed a theoretical analysis of 3D MHD hybrid nanoliquid flow as well as its thermal characteristics and solar applicability. The addition of nano components to the base fluid is thought to upsurge the velocity of the hybrid nanofluid and the efficiency of energy conversion. Alharbi et al.[30] described the flow of a highly conductive trihybrid nanofluid with thermal flux comprising metallic nps along with an extended cylinder with magnetic induction impacts. The magnetic constant and inverse Prandtl number have been found to restrict fluid flow and raise the temperature contour. Jamshed et al.[31] examined the continuous stream of a hybrid ferrofluid and its heat conduction features as it passes over a glossy surface and motor oil. Ahmadian et al.[32] observed the Maxwell hybrid nanoliquid flow moving across two horizontal spinning discs. According to the findings, the disc-expanding action opposes the flow behavior. Zhang et al.[33] addressed the 3D computational formulation of an unstable Ag−MgO/water hybrid peristaltic transport with energy and momentum transfer induced by a moving wavy revolving disc. The topology of a whirling disc is hypothesized to affect velocities and thermal heat transfer in a beneficial way. Sepehrnia et al.[34] addressed the rheologic conduct and active transport through engine oil. Bilal et al.[35] reported the joint upshot of magnetism and electrohydrodynamics on hybrid nanofluids flow. The electric component enhances the velocity boundary layer while decreasing the temperature contour. Pattanaik et al.[36] analyzed the flow characteristics of a 2D conducting hybrid nanofluid passing via an exponentially extending porous substrate. The flow outlines rise as the thermal buoyancy variable increases. The influence of Hall current, magnetic flux, and heat radiation on hybrid nanofluid flow across the top of a rotating disc was investigated by Lv et al.[37] Their goal was to improve the energy propagation rate for mechanical manufacturing applications. Nourinia et al.[38] reviewed the ZnO-CP/MMT hybrid nanoliquid to improve the performance of base fluid for commercial applications by incorporating nanomaterials. Gal et al.[39] performed a numerical analysis of the CNTs and water-based nanoliquid in a 3D cavity with mixed convection. By raising the obstacle opening angle and the CNT volume fraction, an improvement in energy transfer was seen. Recently many researchers have made a significant contribution to the field of hybrid nanofluids.[38−46]

A magnetic dipole is a measurement of a magnet's magnetic intensity and orientation, as well as any other item that generates a magnetic force.[47] Gowda et al.[48] experimented with the magnetic dipole influence on 2D ferromagnetic fluid flow across a flat flexible surface. Kumar et al.[49] addressed the energy allocation through hybrid nanoliquid flow across an extending sheet while accounting for magnetic dipoles. The intensification in the magnetic integrand decreases the velocity

https://doi.org/10.1021/acsomega.2c04600
ACS Omega 2022, 7, 36611−36622

of fluids, whereas the thermal properties of the liquids show the opposite tendency. The efficiency of heat and mass transport slows as the ferromagnetic parameter rises. Gul et al.[50] investigated the hybrid nanocomposites flow moving over an extending sheet, as well as the function of the magnetic dipole on nanofluid flow. Shuaib et al.[51] depicted the nanoliquid flow across two orthogonal whirling discs, with the simultaneous impact of an electromagnetic force on the nanoliquid flow, as well as energy and mass transport properties. Copper oxide nanoparticles have been found to have a good influence on molecular transmitting power and can be employed for refrigeration. Shoaib et al.[52] have devised numerical computing and have assessed a novel hydromagnetic fluid flow model in the context of a magnetic dipole. Isa et al.[53] examined the K_2CO_3−Glycine nanofluid for the dynamical analysis of environmental cleanliness from carbon dioxide. Some recent literature related to fluid flow under the upshot of magnetic dipole has been documented.[54−60]

Nanotechnology has been the subject of research due to its wide range of potential applications in engineering and biomedical fields. The insertion of a trihybrid nanomaterials mixture (Al_2O_3, SiO_2, and TiO_2) in Ellis's liquid is studied in the present analysis within the context of magnetic dipole, heat source, and Darcy Forchhemier medium. The phenomena of fluid flow have been mathematically designed for energy and fluid velocity in the form of a nonlinear system of partial differential equations. The system of Partial differential equations (PDEs) is further simplified to the set of ordinary differential equations (ODEs) through suitable resemblance substitutions. The obtained dimensional equations are mathematically resolved with the help of the semi-analytical technique HAM. In the next section, the flow scenario has been formulated, unraveled, and discoursed.

2. MATHEMATICAL FORMULATION

The heat transition is studied through two-dimensional Ellis's fluid over an extending sheet. The Ellis fluid is immersed along with the engine oil (base fluid). Three different sorts of nano particulates (SiO_2, TiO_2, and Al_2O_3) are dispersed in the engine oil. The wall surface is assumed to be stretchable to generate motion in fluid molecules. The motion in fluidic atoms is generated due to the fluctuation of the wall. The magnetic dipole is supposed in the center and placed horizontally. The flow dynamics are elaborated in Figure 1.

The x-axis and y-axis are taken along the horizontal direction and vertical direction. Thermal energy transfer is considered as absorption and generation into the trihybrid nanofluid. The basic modeled phenomena are articulated as:[49,50]

$$\frac{\partial u}{\partial x} + \frac{\partial u}{\partial y} = 0 \tag{1}$$

$$\rho_{\mathrm{Thnf}}\left(u\frac{\partial u}{\partial x} + v\frac{\partial u}{\partial y}\right) = -\frac{\partial p}{\partial x} + \frac{\partial}{\partial y}\left(\frac{\mu_{\mathrm{Thnf}}}{1 + \left(\frac{1}{\tau_0^2}\frac{\partial u}{\partial y}\right)^{\alpha-1}}\frac{\partial u}{\partial y}\right) + \mu_0 M\frac{\partial H}{\partial x} + \sigma_{\mathrm{Thnf}}(E_0B_0 - B_0^2u) \tag{2}$$

$$(\rho C_p)_{\mathrm{Thnf}}\left(u\frac{\partial T}{\partial x} + v\frac{\partial T}{\partial y}\right) + \left(u\frac{\partial H}{\partial x} + v\frac{\partial H}{\partial y}\right)\mu_0 T\frac{\partial M}{\partial T} = k_{\mathrm{Thnf}}\frac{\partial^2 T}{\partial y^2} - \lambda_2\left(u\frac{\partial u}{\partial x}\frac{\partial T}{\partial x} + v\frac{\partial v}{\partial y}\frac{\partial T}{\partial y} + v\frac{\partial u}{\partial y}\frac{\partial T}{\partial x} + 2uv\frac{\partial^2 T}{\partial x\partial y} + u^2\frac{\partial^2 T}{\partial x^2} + v^2\frac{\partial^2 T}{\partial y^2}\right) + Q_0(T - T_\infty) + \sigma_{\mathrm{Thnf}}(B_0u - E_0)^2 \tau\left(D_B\frac{\partial C}{\partial y}\frac{\partial T}{\partial y} + \frac{D_T}{T_\infty}\left(\frac{\partial T}{\partial y}\right)^2\right), \tag{3}$$

$$u\frac{\partial C}{\partial x} + v\frac{\partial C}{\partial y} = D_B\frac{\partial^2 C}{\partial y^2} + \frac{D_T}{T_\infty}\frac{\partial^2 T}{\partial y^2} - k_1(C - C_\infty) \tag{4}$$

The boundary conditions are

$$u = u_w = sx,\ v = 0,\ T = T_w,\ C = C_w\ at\ y = 0$$
$$u \to 0,\ T \to T_\infty,\ C \to C_\infty at\ y \to \infty \tag{5}$$

The similarity transformations variables are expressed as

$$u = sxf'(\eta),\ v = -\sqrt{s\vartheta_f}f(\eta),\ \frac{T - T_\infty}{T_w - T_\infty} = \theta(\eta),\ \frac{C - C_\infty}{C_w - C_\infty} = \phi(\eta),\ \eta = \sqrt{\frac{s}{\vartheta_f}}y \tag{6}$$

As a result of eqs 6, 1−4 have taken the following form

$$\frac{(1 + (2 - \alpha)(\beta_1 f'')^{\alpha-1})}{(1 + (\beta_1 f'')^{\alpha-1})^2}f''' + \frac{\vartheta_f}{\vartheta_{\mathrm{Thnf}}}(ff'' - f'^2) + \frac{1}{\epsilon}\left[\frac{\sigma_{\mathrm{Thnf}}}{\sigma_f}Ha^2(E_1 - f') - \frac{2\beta\theta}{(\eta + \gamma)^4}\right] = 0 \tag{7}$$

$$\theta'' + \frac{(\rho C_p)_{\mathrm{Thnf}}k_f}{(\rho C_p)_f k_{\mathrm{Thnf}}}\mathrm{Pr}f\theta' + \frac{k_f}{k_{\mathrm{Thnf}}}\frac{\lambda_1 2\beta f(\theta - \varepsilon_1)}{(\eta + \gamma)^3} - \frac{k_f}{k_{\mathrm{Thnf}}}\delta_e Pr(ff'\theta' + f^2\theta'') + \frac{k_f}{k_{Thnf}}\beta\ \mathrm{Pr}\ Ec(\theta - \varepsilon_1)\left[\frac{2f'}{(\eta + \gamma)^4} + \frac{4f}{(\eta + \gamma)^5}\right] + \frac{k_f}{k_{\mathrm{Thnf}}}\mathrm{Pr}(Nb\phi'\theta' + Nt\theta'^2) + \frac{k_f}{k_{\mathrm{Thnf}}}Ht\ \mathrm{Pr}\ \theta + \frac{\sigma_{\mathrm{Thnf}}}{\sigma_f}\frac{k_f}{k_{\mathrm{Thnf}}}Ha^2\ \mathrm{Pr}\ Ec\ (f' - E_1)^2 = 0 \tag{8}$$

$$\phi'' + \frac{Nt}{Nb}\theta'' + \mathrm{Sc}(f\phi' - R_c\phi) = 0 \tag{9}$$

https://doi.org/10.1021/acsomega.2c04600
ACS Omega 2022, 7, 36611−36622

The reduced boundary conditions are

$$f(0) = 0, f'(0) = 1, \theta(0) = 1, \phi(0) = 1$$
$$f'(\infty) = 0, \theta(\infty) = 0, \phi(\infty) = 0 \quad (10)$$

where, $\varepsilon = (1 - \varphi_1)^{2.5}(1 - \varphi_2)^{2.5}(1 - \varphi_3)^{2.5}$

The nondimensional parameters appearing in this study are defined as

$$\beta_1 = \frac{1}{\tau_0^2}\sqrt{\frac{su_w^2}{\vartheta_f}}, Ha^2 = \frac{B_0^2\sigma_f u_w}{\rho_f}, \beta = \frac{\gamma^* M \rho_f \mu_0}{2\pi\mu_f^2}, E_1 = \frac{E_0}{B_0 u_w}, Pr = \frac{\vartheta_f(\rho C_p)_f}{k_f}, Ht = \frac{Q_0}{s(\rho C_p)_f},$$
$$\delta_e = \frac{\lambda_2 s}{(\rho C_p)_f}, Ec = \frac{x}{C_p(T_w - T_\infty)}, Nb = \frac{\tau D_B(C_w - C_\infty)}{\vartheta_f(\rho C_p)_f}, Nb = \frac{\tau D_T(T_w - T_\infty)}{\vartheta_f(\rho C_p)_f}, Sc = \frac{\vartheta_f}{D_B}, R_c = \frac{k_1}{s} \quad (11)$$

3. PHYSICAL QUANTITIES OF INTEREST

The physical quantities of engineering interest are as follows

$$c_f = \frac{\tau_\omega}{\rho_f u_w^2}, N_u = \frac{x q_\omega}{k_f(T_w - T_\infty)} \quad (12)$$

where τ_ω and q_ω are the surface shear stress and heat flux, defined as

$$\tau_\omega = \left[\frac{\mu_{Thnf}}{1 + \left(\frac{1}{\tau_0^2}\frac{\partial u}{\partial y}\right)^{\alpha-1}}\frac{\partial u}{\partial y}\right]_{y=0}, q_\omega = -k_{Thnf}\left(\frac{\partial T}{\partial y}\right)_{y=0} \quad (13)$$

The dimensionless form of eq 11 is

$$Re_x^{1/2}C_f = \frac{1}{\epsilon}\frac{f''(0)}{1 + (\beta_1 f'')^{\alpha-1}}, Re_x^{-1/2}N_u = -\frac{k_{Thnf}}{k_f}\theta'(0) \quad (14)$$

4. SOLUTION METHOD

We should use Homotopy Analysis Method (HAM) with the following processes to rectify eqs 7−9 underneath the constraints of eqs 10. The solutions with the auxiliary factors ħ modify and regulate the solution convergence.

The following are the initial suppositions

$$f_0(\eta) = (1 - e^{-\eta}), \theta_0(\eta) = e^{-\eta}, \phi_0(\eta) = e^{-\eta}, \quad (15)$$

The linear operators are assumed to be $\varpi_f, \varpi_\theta, \theta_\phi$,

$$\varpi_f(f) = f''' - f', \varpi_\theta(\theta) = \theta'' - \theta, \varpi_\phi(\phi) = \phi'' - \phi, \quad (16)$$

which have the following characteristics

$$\varpi_f(c_1 + c_2 e^{-\eta} + c_3 e^{\eta}) = 0, \varpi_\theta(c_4 e^{\eta} + c_5 e^{-\eta}) = 0,$$
$$\varpi_\phi(c_6 e^{\eta} + c_7 e^{-\eta}) = 0, \quad (17)$$

where in general solution $c_i (i = 1-7)$ are constants

The resultant nonlinear operatives N_f, N_θ, N_ϕ, are specified as

$$N_f[f(\eta; p), \theta(\eta; p)] = \frac{\left(1 + (2 - \alpha)\left(\beta_1\frac{\partial^2 f(\eta;p)}{\partial\eta^2}\right)^{\alpha-1}\right)}{\left(1 + \left(\beta_1\frac{\partial^2 f(\eta;p)}{\partial\eta^2}\right)^{\alpha-1}\right)^2}\frac{\partial^3 f(\eta; p)}{\partial\eta^3} + \frac{\vartheta_f}{\vartheta_{Thnf}}\left(f(\eta; p)\frac{\partial^2 f(\eta; p)}{\partial\eta^2} - \left(\frac{\partial f(\eta; p)}{\partial\eta}\right)^2\right) + \frac{1}{\epsilon}\left[\frac{\sigma_{Thnf}}{\sigma_f}Ha^2\left(E_1 - \frac{\partial f(\eta; p)}{\partial\eta}\right) - \frac{2\beta\theta(\eta; p)}{(\eta + \gamma)^4}\right] \quad (18)$$

$$N_\theta[f(\eta; p), \theta(\eta; p), \phi(\eta; p)] = \frac{\partial^2\theta(\eta; p)}{\partial\eta^2} + \frac{(\rho C_p)_{Thnf}k_f}{(\rho C_p)_f k_{Thnf}}Pr f(\eta; p)\frac{\partial\theta(\eta; p)}{\partial\eta} + \frac{k_f}{k_{Thnf}}\frac{\lambda_1 2\beta f(\eta; p)(\theta(\eta; p) - \varepsilon_1)}{(\eta + \gamma)^3} - \frac{k_f}{k_{Thnf}}\delta_e Pr\left(f(\eta; p)\frac{\partial f(\eta; p)}{\partial\eta}\frac{\partial\theta(\eta; p)}{\partial\eta} + (f(\eta; p))^2\frac{\partial^2\theta(\eta; p)}{\partial\eta^2}\right) + \frac{k_f}{k_{Thnf}}\beta PrEc(\theta(\eta; p) - \varepsilon_1)\left[\frac{2}{(\eta + \gamma)^4}\frac{\partial f(\eta; p)}{\partial\eta} + \frac{4f(\eta; p)}{(\eta + \gamma)^5}\right] + \frac{k_f}{k_{Thnf}}Pr\left(Nb\frac{\partial\theta(\eta; p)}{\partial\eta}\frac{\partial\phi(\eta; p)}{\partial\eta} + Nt\left(\frac{\partial\theta(\eta; p)}{\partial\eta}\right)^2\right) + \frac{k_f}{k_{Thnf}}Ht\ Pr\ \theta(\eta; p) + \frac{\sigma_{Thnf}}{\sigma_f}\frac{k_f}{k_{Thnf}}Ha^2\ Pr\ Ec\left(\frac{\partial f(\eta; p)}{\partial\eta} - E_1\right)^2 \quad (19)$$

$$N_\phi[f(\eta; p), \theta(\eta; p), \phi(\eta; p)] = \frac{\partial^2\phi(\eta; p)}{\partial\eta^2} + \frac{N_t}{N_b}\frac{\partial^2\theta(\eta; p)}{\partial\eta^2} - Sc\left(\frac{\partial f(\eta; p)}{\partial\eta}\phi(\eta; p)\right) - Rc\phi(\eta; p) \quad (20)$$

https://doi.org/10.1021/acsomega.2c04600
ACS Omega 2022, 7, 36611−36622

The literature[61−63] describes the fundamental concept of HAM, and the zero-order problems from eqs 7−9 are

$$(1-p)\varpi_f[f(\eta;p)-f_0(\eta)] = p\hbar_f N_f[f(\eta;p),\theta(\eta;p)] \tag{21}$$

$$(1-p)\varpi_\theta[\theta(\eta;p)-\theta_0(\eta)] = p\hbar_\theta N_\theta[f(\eta;p),\theta(\eta;p),\phi(\eta;p)] \tag{22}$$

$$(1-p)\varpi_\phi[\phi(\eta;p)-\phi_0(\eta)] = p\hbar_\phi N_\phi[f(\eta;p),\theta(\eta;p),\phi(\eta;p)] \tag{23}$$

The equivalent boundary conditions are

$$f(\eta;p)|_{\eta=0} = 0,\ \left.\frac{\partial f(\eta;p)}{\partial\eta}\right|_{\eta=0} = 1,\ \left.\frac{\partial f(\eta;p)}{\partial\eta}\right|_{\eta\to\infty} = 0,$$
$$\theta(\eta;p)|_{\eta=0} = 1,\ \theta(\eta;p)|_{\eta\to\infty} = 0,$$
$$\phi(\eta;p)|_{\eta=0} = 1,\ \phi(\eta;p)|_{\eta\to\infty} = 0, \tag{24}$$

where $p\in[0,1]$ denotes the embedding parameter, $\hbar_f$, $\hbar_\theta$, $\hbar_\phi$, are utilized to control the solution's convergence. At $p = 0$ and $p = 1$ we get:

$$f(\eta;1) = f(\eta),\ \theta(\eta;1) = \theta(\eta),\ \phi(\eta;1) = \phi(\eta), \tag{25}$$

Inflating $f(\eta;p)$,$\theta(\eta;p)$,$\phi(\eta;p)$,$\chi(\eta;p)$ in Taylor's series about $p = 0$

$$f(\eta;p) = f_0(\eta) + \sum_{m=1}^{\infty} f_m(\eta)p^m,$$
$$\theta(\eta;p) = \theta_0(\eta) + \sum_{m=1}^{\infty} \theta_m(\eta)p^m,$$
$$\phi(\eta;p) = \phi_0(\eta) + \sum_{m=1}^{\infty} \phi_m(\eta)p^m. \tag{26}$$

where

$$f_m(\eta) = \frac{1}{m!}\left.\frac{\partial f(\eta;p)}{\partial\eta}\right|_{p=0},\ \theta_m(\eta) = \frac{1}{m!}\left.\frac{\partial\theta(\eta;p)}{\partial\eta}\right|_{p=0},$$
$$\phi_m(\eta) = \frac{1}{m!}\left.\frac{\partial\phi(\eta;p)}{\partial\eta}\right|_{p=0}, \tag{27}$$

The secondary restrictions $\hbar_f$, $\hbar_\theta$, $\hbar_\phi$ are selected in such a tactic that the series (26) converges at$p = 1$; exchanging $p = 1$ in eq 26, we acquire

$$f(\eta) = f_0(\eta) + \sum_{m=1}^{\infty} f_m(\eta),$$
$$\theta(\eta) = \theta_0(\eta) + \sum_{m=1}^{\infty} \theta_m(\eta),$$
$$\phi(\eta) = \phi_0(\eta) + \sum_{m=1}^{\infty} \phi_m(\eta). \tag{28}$$

The mth-order problem fulfills the following:

$$\varpi_f[f_m(\eta) - \chi_m f_{m-1}(\eta)] = \hbar_f R_m^f(\eta),$$
$$\varpi_\theta[\theta_m(\eta) - \chi_m \theta_{m-1}(\eta)] = \hbar_\theta R_m^\theta(\eta),$$
$$\varpi_\varphi[\varphi_m(\eta) - \chi_m \varphi_{m-1}(\eta)] = \hbar_\varphi R_m^\varphi(\eta). \tag{29}$$

The corresponding boundary conditions are

$$f_m(0) = f_m'(0) = \theta_m(0) = \phi_m(0) = 0$$
$$f_m'(\infty) = \theta_m(\infty) = \phi_m(\infty) = 0 \tag{30}$$

Here

$$R_m^f(\eta) = \frac{(1+(2-\alpha)(\beta_1 f_{m-1}'')^{\alpha-1})}{(1+(\beta_1 f_{m-1}'')^{\alpha-1})^2} f_{m-1}''' + \frac{\vartheta_f}{\vartheta_{Thnf}}\left(\sum_{k=0}^{m-1} f_{m-1-k}f_k'' - \sum_{k=0}^{m-1} f_{m-1-k}'f_k'\right) + \frac{1}{\epsilon}\left[\frac{\sigma_{Thnf}}{\sigma_f}Ha^2(E_1 - f_{m-1}') - \frac{2\beta\theta(\eta;p)}{(\eta+\gamma)^4}\theta_{m-1}\right] \tag{31}$$

$$R_m^\theta(\eta) = \theta_{m-1}'' + \frac{(\rho C_p)_{Thnf}k_f}{(\rho C_p)_f k_{Thnf}}\Pr\sum_{k=0}^{m-1} f_{m-1-k}\theta_k' + \frac{k_f}{k_{Thnf}}\frac{\lambda_1 2\beta f(\eta;p)(\sum_{k=0}^{m-1} f_{m-1-k}\theta_k - \varepsilon_1 f_{m-1})}{(\eta+\gamma)^3} - \frac{k_f}{k_{Thnf}}\delta_e\Pr\left(\sum_{k=0}^{m-1} f_{m-1-k}\sum_{l=0}^{k} f_{k-1}'\theta_1' + \sum_{k=0}^{m-1} f_{m-1-k}\sum_{l=0}^{k} f_{k-1}\theta_1''\right) + \frac{k_f}{k_{Thnf}}\beta\Pr Ec(\theta_{m-1} - \varepsilon_1)\left[\frac{2}{(\eta+\gamma)^4}f_{m-1}' + \frac{4f(\eta;p)}{(\eta+\gamma)^5}f_{m-1}\right] + \frac{k_f}{k_{Thnf}}\Pr\left(Nb\sum_{k=0}^{m-1}\theta_{m-1-k}'\phi_k' + Nt\sum_{k=0}^{m-1}\theta_{m-1-k}'\theta_k'\right) + \frac{k_f}{k_{Thnf}}Ht\ \Pr\theta_{m-1} + \frac{\sigma_{Thnf}}{\sigma_f}\frac{k_f}{k_{Thnf}}Ha^2\Pr Ec(f_{m-1}' - E_1)^2 \tag{32}$$

$$R_m^\phi(\eta) = \phi_{m-1}'' + \frac{N_t}{N_b}\theta_{m-1}'' - Sc\left(\sum_{k=0}^{m-1} f_{m-1-k}'\phi_k\right) - Rc\phi_{m-1} \tag{33}$$

where $\chi_m = \begin{cases} 0, & \text{if } p \le 1 \\ 1, & \text{if } p > 1 \end{cases}$

https://doi.org/10.1021/acsomega.2c04600
ACS Omega 2022, 7, 36611−36622

5. RESULTS AND DISCUSSION

This section expresses the physical mechanism and trend behind each Figure and Table. Figure 1a,b illustrates the flow configuration under the influence of magnetic dipole and synthesis of ternary nanofluid with the dispersion of Al_2O_3, SiO_2, and TiO_2 nanoparticles in engine oil.

Figures 2−6 display the velocity outlines $f'(\eta)$ versus the influence of fluid parameter β_1, ferrohydrodynamic interaction term β, Hartman number Ha^2, magnetic dipole γ, and local electric parameter E_1, respectively. Figures 2 and 3 determine that the velocity contour improves with the influence of fluid parameter β_1 while diminishes by the action of ferrohydrodynamic interaction term β. Physically, the stretching velocity of the plate intensifies with the impact of fluid constraint, which reassures the fluid particles to stream fast, as a result, the velocity field $f'(\eta)$ improves as presented in Figure 2. The magnetic effect and density of fluid enhance the variation of the ferrohydrodynamic interaction factor. Actually, the magnetic effect (due to Lorentz force) and density of the fluid, both stipulate hurdles to the flow field, which bases the decline of momentum boundary layer $f'(\eta)$.

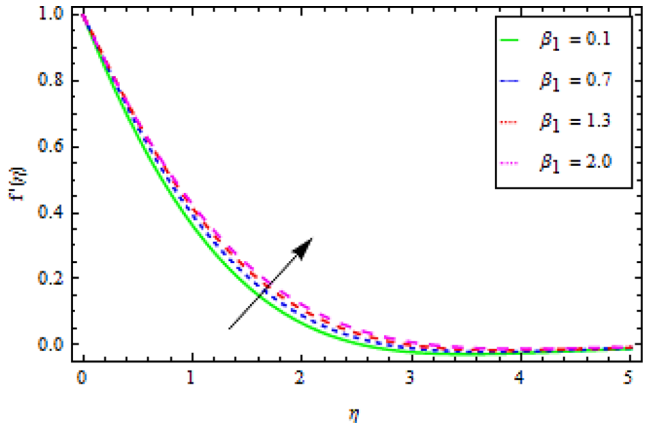

Figure 2. Velocity outlines $f'(\eta)$ versus the fluid parameter β_1.

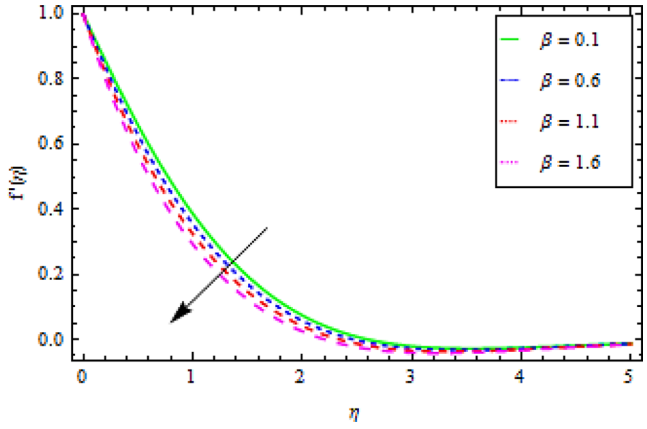

Figure 3. Velocity outlines $f'(\eta)$ versus the ferrohydrodynamic interaction number β.

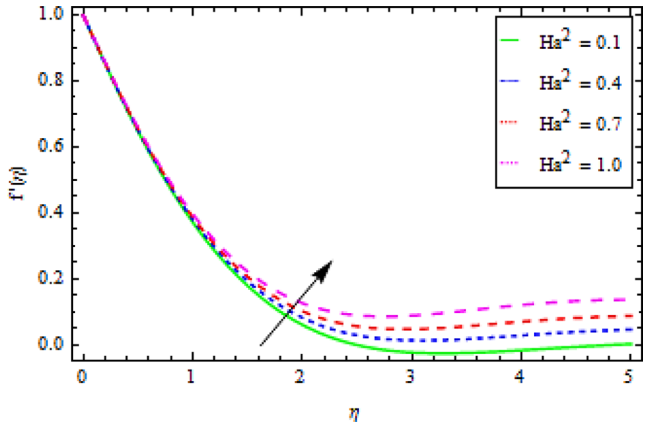

Figure 4. Velocity outlines $f'(\eta)$ versus the Hartman number Ha^2.

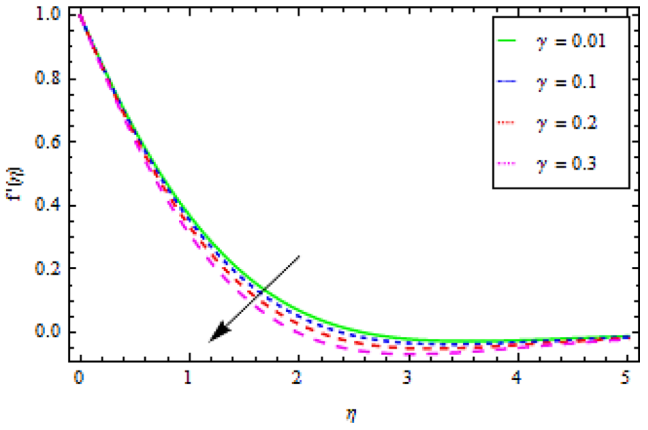

Figure 5. Velocity outlines $f'(\eta)$ versus the magnetic dipole γ.

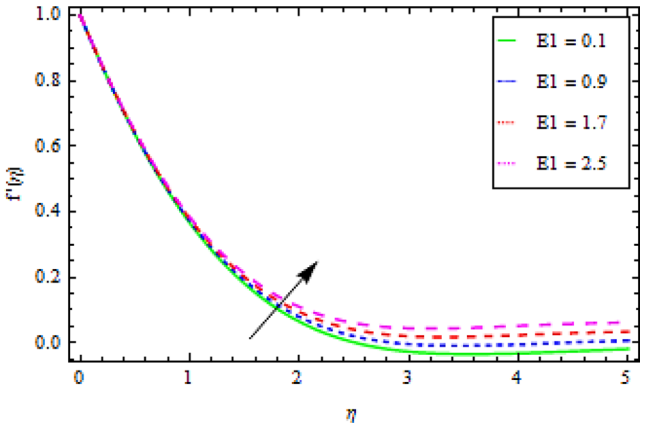

Figure 6. Velocity outlines $f'(\eta)$ versus the local electric parameter E_1.

Figures 4 and 5 govern that the velocity curve $f'(\eta)$augments with the outcome of Hartman number Ha^2, while degenerating with the consequence of the magnetic dipole parameter. Physically, the rising influence of the Hartmann number boosts the stretching velocity of the vertical plate as well as lessens the density of base fluid, which reasons for such a state, as observed in Figure 4. The magnetic dipole generates resistive effects, which contest the flow stream and drops its velocity $f'(\eta)$, as publicized in Figure 5. Figure 6 shows that the velocity profile magnifies with the growing upshot of local electric constraint E_1. The magnetic effect and stretching velocity of the vertical surface both exposed an inverse trend against the electric force, as a product the velocity field $f'(\eta)$ boosts.

Figures 7−13 highlighted the behavior of energy contourθ-(η) versus the upshot of ferrohydrodynamic interaction number β, Hartman number Ha^2, thermal relaxation parameter

https://doi.org/10.1021/acsomega.2c04600
ACS Omega 2022, 7, 36611−36622

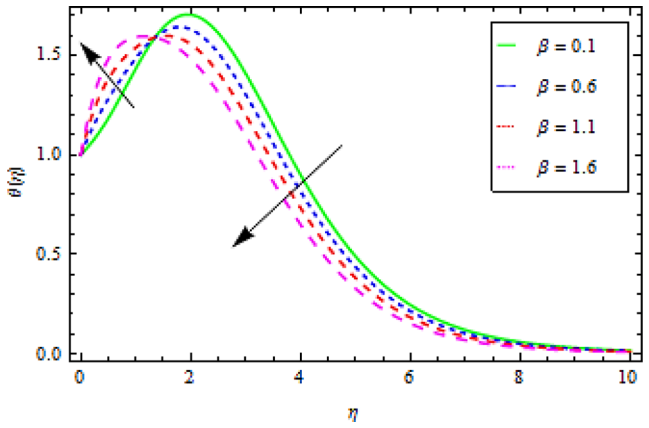

Figure 7. Energy outlines $\theta(\eta)$ versus the ferrohydrodynamic interaction number β.

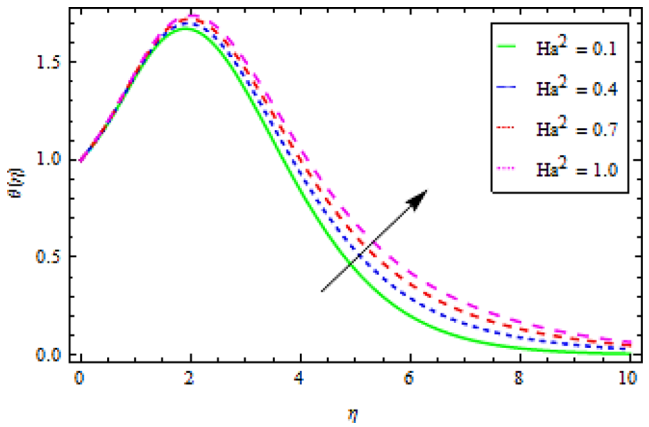

Figure 8. Energy outlines $\theta(\eta)$ versus the Hartman number Ha^2.

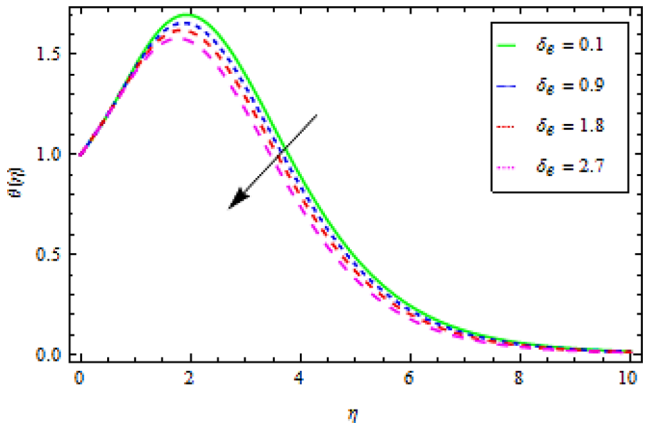

Figure 9. Energy outlines $\theta(\eta)$ versus the thermal relaxation parameter δ_e.

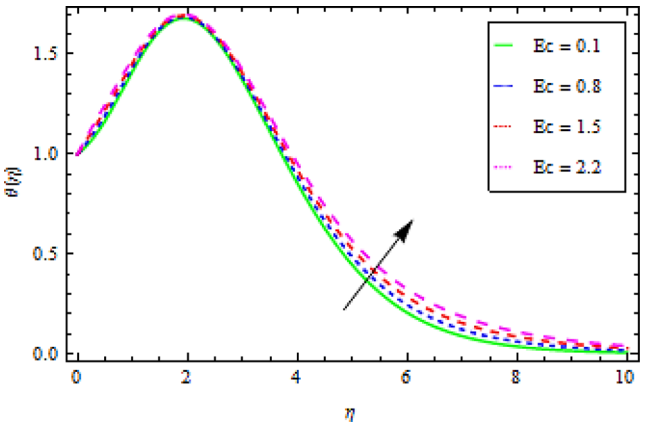

Figure 10. Energy outlines $\theta(\eta)$ versus the Eckert number Ec.

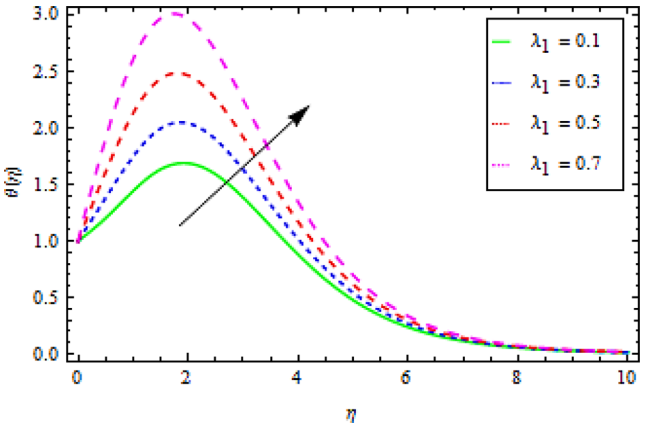

Figure 11. Energy outlines $\theta(\eta)$ versus the viscous dissipation term λ_1.

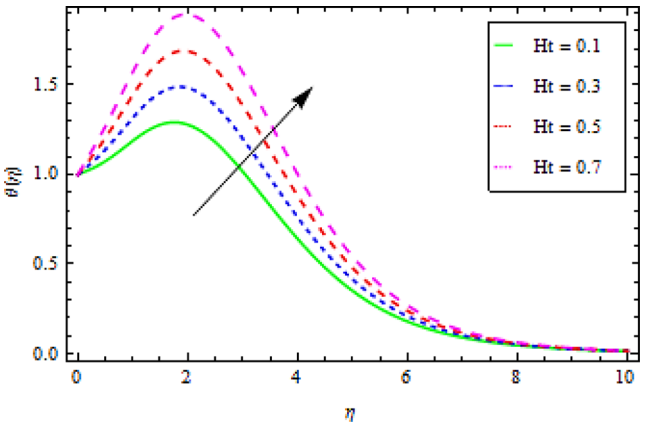

Figure 12. Energy outlines $\theta(\eta)$ versus the heat source number Ht.

δ_e, Eckert number Ec, viscous dissipation term λ_1, heat source number Ht, and local electric parameter E_1, respectively. Figures 7 and 8 exposed that the energy field diminutions with the influence of ferrohydrodynamic interaction factor augments with the difference of Hartman number Ha^2. As discussed earlier, the magnetic effect and density of fluid improve versus the variation of the ferrohydrodynamic interaction factor, which resists the flow field and generates friction force; as a result, the fluid energy field $\theta(\eta)$declines. On the other hand, the rising frequency of the Hartmann number expands the energy profile $\theta(\eta)$as exposed in Figure 8. Figures 9 and 10 uncovered that the energy field contracts with the impact of thermal relaxation parameter δ_e and enriches with the variation of Eckert number Ec. Additional heat is produced due to the upshot of the Eckert number because the specific heat capacity of fluid declines with the influence of the Eckert number, which causes an elevation in the energy profile $\theta(\eta)$.

Figures 11 and 12 exposed that the energy profile enriches with the influence of thermal viscous dissipation term λ_1 and heat source number Ht. The heat source parameter works as a

https://doi.org/10.1021/acsomega.2c04600
ACS Omega 2022, 7, 36611−36622

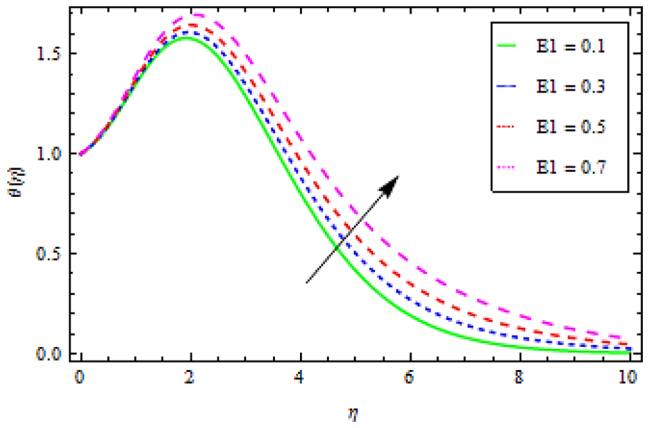

Figure 13. Energy outlines $\theta(\eta)$ versus the local electric parameter E_1.

heat generating agent in the fluid, so the rising impact of the heat source term boosts the energy distribution as shown in Figure 12. Figure 13 shows that the action of the local electric parameter also magnifies the energy profile because the magnetic effect and stretching velocity of the vertical surface both exposed an inverse relation to the electric force, and as a consequence, the energy field $\theta(\eta)$ boosts.

Figures 14−17 reported the compartment of concentration contour $\phi(\eta)$ versus the upshot of Schmidt number *Sc*,

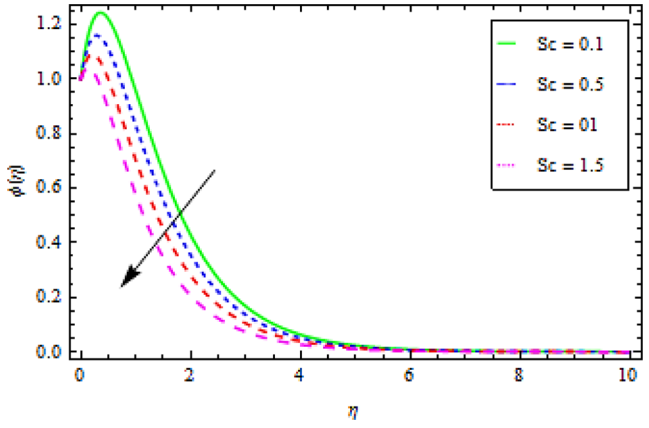

Figure 14. Concentration outlines $\phi(\eta)$ versus the Schmidt number *Sc*.

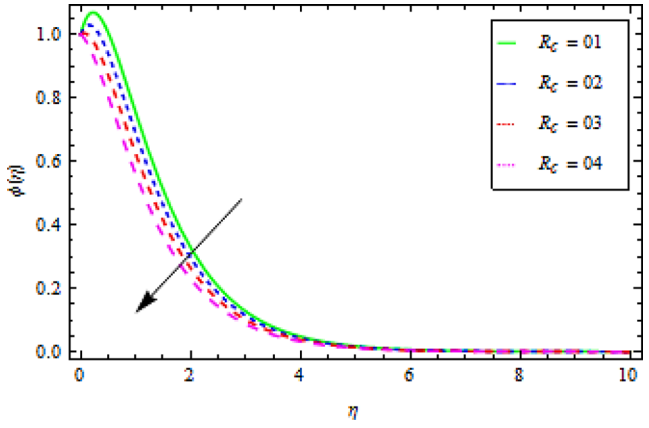

Figure 15. Concentration outlines $\phi(\eta)$ versus the chemical reaction parameter R_c.

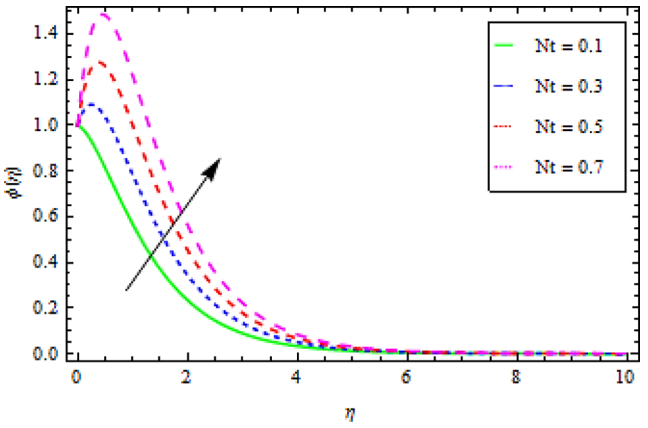

Figure 16. Concentration outlines $\phi(\eta)$ versus the thermophoresis effect Nt.

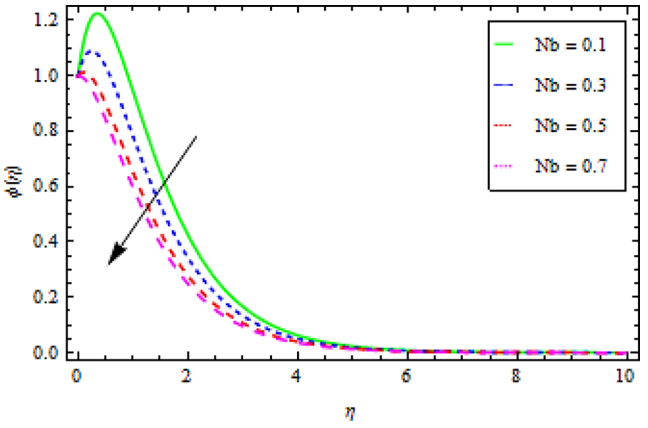

Figure 17. Concentration outlines $\phi(\eta)$ versus the Brownian motion Nb.

chemical reaction parameter R_c, thermophoresis effect Nt, and Brownian motion *Nb*, respectively. Figures 14 and 15 show that the mass transfer rate reduces with the effect of the Schmidt number and chemical reaction factor. Physically, the kinetic viscosity of ternary nanofluid enhances, while the molecular diffusion declines with the action of the Schmidt number, which results in the retardation of mass transition rate. Figures 16 and 17 revealed that the concentration outlines dimming with the upshot of the thermophoresis effect and augments with the action of the Brownian motion *Nb*. The Brownian motion of fluid particles inside the fluid generates a retarding effect, which opposes the moving fluid; eventually, the mass transmission rate $\phi(\eta)$ reduces.

Tables 1 and 2 expressed the experimental values and basic thermophysical characteristics of ternary nanoparticles and engine oil, respectively. Tables 3 and 4 revealed the statistical results of skin friction $\mathrm{Re}_x^{1/2}C_f$and Nusselt number

Table 1. Investigational Values of Al_2O_3, SiO_2, TiO_2, and Engine Oil[54]

	K	σ	ρ
Engine oil	0.144	0.125×10^{-11}	884
Al_2O_3	32.9	5.96×10^{7}	6.310
TiO_2	8.953	2.4×10^{6}	4.250
SiO_2	1.4013	3.5×10^{6}	2.270

https://doi.org/10.1021/acsomega.2c04600
ACS Omega 2022, 7, 36611−36622

Table 2. Thermochemical Properties of Ternary Hybrid Nanofluids[54]

viscosity	$\frac{\mu_{Thnf}}{\mu_f} = \frac{1}{(1-\phi_{Al_2O_3})^{2.5}(1-\phi_{TiO_2})^{2.5}(1-\phi_{SiO_2})^{2.5}}$,
density	$\frac{\rho_{Thnf}}{\rho_f} = (1-\phi_{TiO_2})\left[(1-\phi_{TiO_2})\left\{(1-\phi_{SiO_2}) + \phi_{SiO_2}\frac{\rho_{SiO_2}}{\rho_f}\right\} + \phi_{TiO_2}\frac{\rho_{TiO_2}}{\rho_f}\right] + \phi_{Al_2O_3}\frac{\rho_{Al_2O_3}}{\rho_f}$,
specific heat	$\frac{(\rho cp)_{Thnf}}{(\rho cp)_f} = \phi_{Al_2O_3}\frac{(\rho cp)_{Al_2O_3}}{(\rho cp)_f} + (1-\phi_{Al_2O_3})\left[(1-\phi_{TiO_2})\left\{(1-\phi_{SiO_2}) + \phi_{SiO_2}\frac{(\rho cp)_{SiO_2}}{(\rho cp)_f}\right\} + \phi_{TiO_2}\frac{(\rho cp)_{TiO_2}}{(\rho cp)_f}\right]$
thermal conduction	$\left.\begin{aligned}\frac{k_{Thnf}}{k_{hnf}} &= \left(\frac{k_{SiO_2} + 2k_{hnf} - 2\phi_{SiO_2}(k_{hnf} - k_{SiO_2})}{k_{SiO_2} + 2k_{hnf} + \phi_{SiO_2}(k_{hnf} - k_{SiO_2})}\right), \frac{k_{hnf}}{k_{nf}} \\ &= \left(\frac{k_{TiO_2} + 2k_{nf} - 2\phi_{TiO_2}(k_{nf} - k_{TiO_2})}{k_{TiO_2} + 2k_{nf} + \phi_{TiO_2}(k_{nf} - k_{TiO_2})}\right), \\ \frac{k_{nf}}{k_f} &= \left(\frac{k_{Al_2O_3} + 2k_f - 2\phi_{Al_2O_3}(k_f - k_{Al_2O_3})}{k_{Al_2O_3} + 2k_f + \phi_{Al_2O_3}(k_f - k_{Al_2O_3})}\right),\end{aligned}\right\}$
electrical conductivity	$\left.\begin{aligned}\frac{\sigma_{Thnf}}{\sigma_{hnf}} &= \left(1 + \frac{3\left(\frac{\sigma_{SiO_2}}{\sigma_{hnf}} - 1\right)\phi_{SiO_2}}{\left(\frac{\sigma_{SiO_2}}{\sigma_{hnf}} + 2\right) - \left(\frac{\sigma_{SiO_2}}{\sigma_{hnf}} - 1\right)\phi_{SiO_2}}\right), \frac{\sigma_{hnf}}{\sigma_{nf}} \\ &= \left(1 + \frac{3\left(\frac{\sigma_{TiO_2}}{\sigma_{nf}} - 1\right)\phi_{TiO_2}}{\left(\frac{\sigma_{TiO_2}}{\sigma_{nf}} + 2\right) - \left(\frac{\sigma_{TiO_2}}{\sigma_{nf}} - 1\right)\phi_{TiO_2}}\right), \\ \frac{\sigma_{nf}}{\sigma_f} &= \left(1 + \frac{3\left(\frac{\sigma_{Al_2O_3}}{\sigma_f} - 1\right)\phi_{Al_2O_3}}{\left(\frac{\sigma_{Al_2O_3}}{\sigma_f} + 2\right) - \left(\frac{\sigma_{Al_2O_3}}{\sigma_f} - 1\right)\phi_{Al_2O_3}}\right).\end{aligned}\right\}$

Table 3. The Quantitive Outputs of Skin Friction $Re_x^{1/2}C_f$ Versus Different Physical Constraints

β_1	β	Ha^2	E_1	$Re_x^{1/2}C_f$
0.1				−0.59661753
0.3				−0.68863742
0.5				−0.81688495
	0.1			−0.63914198
	0.3			−0.69008225
	0.5			−0.74219394
		0.1		−0.68637734
		0.3		−0.68498865
		0.5		−0.68221483
			0.1	−0.68659026
			0.3	−0.68629669
			0.5	−0.68600318

Table 4. The Statistical Outputs of Nusselt Number $Re_x^{-1/2}N_u$ Versus Different Physical Constraints

δ_e	Ec	Ht	E_1	$Re_x^{-1/2}N_u$
0.1				−0.95874128
0.3				−0.82782823
0.5				−0.69691517
	0.1			−0.76942363
	0.3			−0.78889183
	0.5			−0.80836003
		0.1		−0.10917382
		0.3		−0.45876692
		0.5		−0.80836003
			0.1	−0.8044098
			0.3	−0.80836003
			0.5	−0.82646483

$Re_x^{-1/2}N_u$versus physical interest entities, respectively. It can be perceived that the rising values of the Hartmann number and electric parameter decline the skin friction, while the influence of the ferrohydrodynamic interaction factor boosts the tendency of skin friction. From Table 4, It can be observed that the upshot of the Eckert and Hartmann number reduces the Nusselt number.

6. CONCLUSIONS

We have studied the augmentation of energy transfer in trihybrid Ellis nanofluid flow when a magnetic dipole passes over a vertical surface. The velocity and heat transportation has been examined in the presence of the electromagnetic effect and heat source/sink. The phenomena of fluid flow have been

https://doi.org/10.1021/acsomega.2c04600
ACS Omega 2022, 7, 36611−36622

mathematically designed for energy and fluid velocity in the form of a nonlinear system of PDEs. The system of PDEs is further refined to the set of ODEs through suitable resemblance substitutions. The obtained dimensional equations are numerically answered with the help of HAM. The key findings are:

1. The velocity outline enhances with the effect of fluid parameter β_1, while diminish by the action of the ferrohydrodynamic interaction term β.
2. The accumulation of Al_2O_3, SiO_2, and TiO_2 nanomaterials to the base fluid "engine oil" advances its momentum and energy profiles.
3. The velocity curve $f'(\eta)$ augments with the outcome of electric constraint E_1 and Hartman numberHa^2 while degenerates as a consequence of the magnetic dipole parameter.
4. Energy field diminutions with the influence of the ferrohydrodynamic interaction factor but augments with the difference of the Hartman number Ha^2.
5. The energy field contracts with the impact of the thermal relaxation parameter δ_e and boosts with the variation of the Eckert number Ec.
6. The energy profile augments with the influence of the electric parameter, thermal viscous dissipation term λ_1, and heat source number Ht.
7. The mass transfer rate reduces with the effect of the Schmidt number and chemical reaction factor.
8. The concentration outlines dimming with the upshot of the thermophoresis effect and augments with the action of Brownian motion Nb.

AUTHOR INFORMATION

Corresponding Authors

Zahir Shah − *Department of Mathematical Sciences, University of Lakki Marwat, Lakki Marwat 28420 Khyber Pakhtunkhwa, Pakistan;* orcid.org/0000-0002-5539-4225; Email: Zahir@ulm.edu.pk

Poom Kumam − *Center of Excellence in Theoretical and Computational Science (TaCS-CoE) & KMUTTFixed Point Research Laboratory, Room SCL 802 Fixed Point Laboratory, Science Laboratory Building, Departments of Mathematics, Faculty of Science, King Mongkut's University of Technology Thonburi (KMUTT), Bangkok 10140, Thailand; Department of Medical Research, China Medical University Hospital, China Medical University, Taichung 40402, Taiwan*; Email: poom.kum@kmutt.ac.th

Authors

Muhammad Rooman − *Department of Mathematical Sciences, University of Lakki Marwat, Lakki Marwat 28420 Khyber Pakhtunkhwa, Pakistan*

Anwar Saeed − *Department of Mathematics, Faculty of Science, King Mongkut's University of Technology Thonburi (KMUTT), Bangkok 10140, Thailand;* orcid.org/0000-0003-1566-6457

Ahmed Alshehri − *Department of Mathematics, Faculty of Sciences, King Abdulaziz University, Jeddah 21589, Saudi Arabia*

Saeed Islam − *Department of Mathematics, Abdul Wali Khan University, Mardan 23200 Khyber Pakhtunkhwa, Pakistan*

Panawan Suttiarporn − *Faculty of Science, Energy and Environment, King Mongkut's University of Technology North Bangkok, Rayong 21120, Thailand*

Complete contact information is available at: https://pubs.acs.org/10.1021/acsomega.2c04600

Funding

"This research was funded by National Science, Research and Innovation Fund (NSRF), King Mongkut's University of Technology North Bangkok with Contract no. KMUTNB-FF-66-61"

Notes

The authors declare no competing financial interest.

NOMENCLATURE

B_0	magnetic field intensity ($A\ m^{-1}$)
C	concentration
D_T	thermophoretic diffusion coefficient
E_1	local electric parameter
k_1	chemical reaction rate
H	Magnetic field
M	magnetization
Nt	thermophoresis parameter
Q_0	heat source number
Re_x	local Reynolds number
T	temperature of fluid
x,y	coordinates axis (m)

GREEK LETTERS

α,τ_0^2	material parameter
β	ferrohydrodynamic interaction number
γ	strength of the magnetic dipole
ε_1	ratio parameter
θ	dimensionless temperature
λ_2	thermal relaxation time
ϑ	kinematic viscosity
ρc_p	heat capacity
ϕ_1,ϕ_2,ϕ_3	volume fraction

SUBSCRIPTS

f	fluid
hnf	hybrid nanofluid
C_p	specific heat transfer ($J\ kg^{-1}\ K^{-1}$)
D_B	Brownian diffusion coefficient
E_0	electric field intensity
Ec	Eckert number
k	thermal conductivity ($W\ m^{-1}\ K^{-1}$)
Ha^2	Hartman number
Nb	Brownian motion parameter
Pr	Prandtl number
R_c	chemical reaction parameter
Sc	Schmidt number
u,v	velocity components ($m\ s^{-1}$)
α_1	temperature ratio
β_1	fluid parameter
δ_e	thermal relaxation parameter
η	independent coordinate
λ_1	viscous dissipation number
μ_0	magnetic permeability
ρ	density ($kg\ m^{-3}$)
σ	electrical conductivity
bf	base fluid
Thnf	ternary hybrid nanofluid

https://doi.org/10.1021/acsomega.2c04600
ACS Omega 2022, 7, 36611−36622

REFERENCES

(1) Algehyne, E. A.; Alhusayni, Y. Y.; Tassaddiq, A.; Saeed, A.; Bilal, M. The study of nanofluid flow with motile microorganism and thermal slip condition across a vertical permeable surface. *Waves in Random and Complex Media* **2022**, 1−18.

(2) Hosseinzadeh, K.; Roghani, S.; Asadi, A.; Mogharrebi, A.; Ganji, D. D. Investigation of micropolar hybrid ferrofluid flow over a vertical plate by considering various base fluid and nanoparticle shape factor. *Int. J. Numer. Methods Heat Fluid Flow* **2021**, *31*, 402−417.

(3) Janardhana Reddy, G.; Kumar, M.; Anwar Beg, O. Effect of temperature dependent viscosity on entropy generation in transient viscoelastic polymeric fluid flow from an isothermal vertical plate. *Phys. A Stat. Mech. its Appl.* **2018**, *510*, 426−445.

(4) Sehra.; et al. Convection heat mass transfer and MHD flow over a vertical plate with chemical reaction, arbitrary shear stress and exponential heating. *Sci. Reports* **2021**, 1−11.

(5) Kumar, M. A.; Reddy, Y. D.; Goud, B. S.; Rao, V. S. Effects of soret, dufour, hall current and rotation on MHD natural convective heat and mass transfer flow past an accelerated vertical plate through a porous medium. *Int. J. Thermofluids* **2021**, *9*, 100061.

(6) Algehyne, E. A.; et al. Numerical simulation of bioconvective Darcy Forchhemier nanofluid flow with energy transition over a permeable vertical plate. *Sci. Reports* **2022**, *12*, 1−12.

(7) Dadheech, A.; Parmar, A.; Agrawal, K.; Al-Mdallal, Q.; Sharma, S. Second law analysis for MHD slip flow for Williamson fluid over a vertical plate with Cattaneo-Christov heat flux. *Case Stud. Therm. Eng.* **2022**, *33*, 101931.

(8) Kodi, R.; Mopuri, O.; Sree, S.; Konduru, V. Investigation of MHD Casson fluid flow past a vertical porous plate under the influence of thermal diffusion and chemical reaction. *Heat Transf* **2022**, *51*, 377−394.

(9) Shah, N. A.; Yook, S. J.; Tosin, O. Analytic simulation of thermophoretic second grade fluid flow past a vertical surface with variable fluid characteristics and convective heating. *Sci. Reports* **2022**, *12*, 1−17.

(10) Shah, N. A.; Wakif, A.; El-Zahar, E. R.; Thumma, T.; Yook, S. J. Heat transfers thermodynamic activity of a second-grade ternary nanofluid flow over a vertical plate with Atangana-Baleanu time-fractional integral. *Alexandria Eng. J.* **2022**, *61*, 10045−10053.

(11) Hussain, S. M.; et al. Effectiveness of Nonuniform Heat Generation (Sink) and Thermal Characterization of a Carreau Fluid Flowing across a Nonlinear Elongating Cylinder: A Numerical Study. *ACS Omega* **2022**, *7*, 25309−25320.

(12) Khan, U.; Zaib, A.; Pop, I.; Abu Bakar, S.; Ishak, A. Unsteady micropolar hybrid nanofluid flow past a permeable stretching/shrinking vertical plate. *Alexandria Eng. J.* **2022**, *61*, 11337−11349.

(13) Arulmozhi, S.; et al. Heat and mass transfer analysis of radiative and chemical reactive effects on MHD nanofluid over an infinite moving vertical plate. *Results Eng* **2022**, *14*, 100394.

(14) Venkata Ramudu, A. C.; Anantha Kumar, K.; Sugunamma, V.; Sandeep, N. Impact of Soret and Dufour on MHD Casson fluid flow past a stretching surface with convective−diffusive conditions. *J. Therm. Anal. Calorim.* **20212021**, *147*, 2653−2663.

(15) Raghunath, K.; Gulle, N.; Vaddemani, R. R.; Mopuri, O. Unsteady MHD fluid flow past an inclined vertical porous plate in the presence of chemical reaction with aligned magnetic field, radiation, and Soret effects. *Heat Transf* **2022**, *51*, 2742−2760.

(16) Bhatti, M. M.; Ellahi, R.; Hossein Doranehgard, M. Numerical study on the hybrid nanofluid (Co3O4-Go/H2O) flow over a circular elastic surface with non-Darcy medium: Application in solar energy. *J. Mol. Liq.* **2022**, *361*, 119655.

(17) Bhatti, M. M.; Öztop, H. F.; Ellahi, R.; Sarris, I. E.; Doranehgard, M. H. Insight into the investigation of diamond (C) and Silica (SiO2) nanoparticles suspended in water-based hybrid nanofluid with application in solar collector. *J. Mol. Liq.* **2022**, *357*, 119134.

(18) Kheyfets, V. O.; Kieweg, S. L. Gravity-Driven Thin Film Flow of an Ellis Fluid. *J. Nonnewton. Fluid Mech.* **2013**, *202*, 88.

(19) Javed, M. A.; Ali, N.; Sajid, M. A theoretical analysis of the calendering of Ellis fluid. *J. Plast. Film Sheeting* **2016**, *33*, 207−226.

(20) Celli, M.; Barletta, A.; Brandão, P. V. Rayleigh−Bénard Instability of an Ellis Fluid Saturating a Porous Medium. *Transp. Porous Media* **2021**, *138*, 679−692.

(21) Sajid, M.; Rooman, M.; Ali, N.; Sadiq, M. N. Flow of the Ellis Fluid in the Renal Tubule. *J. Appl. Mech. Tech. Phys.* **2021**, *622*, 292−299.

(22) Rooman, M.; Jan, M. A.; Shah, Z.; Alzahrani, M. R. Entropy generation and nonlinear thermal radiation analysis on axisymmetric MHD Ellis nanofluid over a horizontally permeable stretching cylinder. *Waves in Random and Complex Media* **2022**, *0*, 1−15.

(23) Shah, R. A.; Asghar, Z.; Ali, N. Mathematical modeling related to bacterial gliding mechanism at low Reynolds number with Ellis Slime. *Eur. Phys. J. Plus* **2022**, *137*, 1−12.

(24) Gul, T.; Bilal, M.; Shuaib, M.; Mukhtar, S.; Thounthong, P. Thin film flow of the water-based carbon nanotubes hybrid nanofluid under the magnetic effects. *Heat Transf* **2020**, *49*, 3211−3227.

(25) Alrabaiah, H.; Bilal, M.; Khan, M. A.; Muhammad, T.; Legas, E. Y. Time fractional model of electro-osmotic Brinkman-type nanofluid with heat generation and chemical reaction effects: application in cleansing of contaminated water. *Sci. Reports* **2021**, *11*, 1−19.

(26) Bilal, M.; et al.*The parametric computation of nonlinear convection magnetohydrodynamic nanofluid flow with internal heating across a fixed and spinning disk*; Taylor & Francis, 2022.

(27) Elattar, S.; et al. Computational assessment of hybrid nanofluid flow with the influence of hall current and chemical reaction over a slender stretching surface. *Alexandria Eng. J.* **2022**, *61*, 10319−10331.

(28) Yahya, A. U.; et al. Thermal charactristics for the flow of Williamson hybrid nanofluid (MoS2 + ZnO) based with engine oil over a streched sheet. *Case Stud. Therm. Eng.* **2021**, *26*, 101196.

(29) Rehman, A.; Saeed, A.; Bilal, M. Analytical study of three-dimensional MHD hybrid nanofluid flow along with thermal characteristics and radiative solar energy. *Waves in Random and Complex Media* **2022**, 1−15.

(30) Alharbi, K. A. M.; et al. Computational Valuation of Darcy Ternary-Hybrid Nanofluid Flow across an Extending Cylinder with Induction Effects. *Micromachines* **2022**, *13*, 588.

(31) Jamshed, W.; et al. Entropy Amplified solitary phase relative probe on engine oil based hybrid nanofluid. *Chinese J. Phys.* **2022**, *77*, 1654−1681.

(32) Ahmadian, A.; Bilal, M.; Khan, M. A.; Asjad, M. I. The non-Newtonian maxwell nanofluid flow between two parallel rotating disks under the effects of magnetic field. *Sci. Reports* **2020**, *10*, 1−14.

(33) Zhang, X. H.; et al. The parametric study of hybrid nanofluid flow with heat transition characteristics over a fluctuating spinning disk. *PLoS One* **2021**, *16*, No. e0254457.

(34) Sepehrnia, M.; Mohammadzadeh, K.; Veyseh, M. M.; Agah, E.; Amani, M. Rheological behavior of engine oil based hybrid nanofluid containing MWCNTs and ZnO nanopowders: Experimental analysis, developing a novel correlation, and neural network modeling. *Powder Technol.* **2022**, *404*, 117492.

(35) Bilal, M.; Gul, T.; Alsubie, A.; Ali, I. Axisymmetric hybrid nanofluid flow with heat and mass transfer amongst the two gyrating plates. *ZAMM - J. Appl. Math. Mech. / Zeitschrift für Angew. Math. und Mech.* **2021**, *101*, No. e202000146.

(36) Pattnaik, P. K., Mishra, S.; Baag, S.*Heat transfer analysis on Engine oil-based hybrid nanofluid past an exponentially stretching permeable surface with Cu/Al2O3 additives*; Proceedings of the Institution of Mechanical Engineers. 2022.

(37) Lv, Y. P.; et al. Numerical approach towards gyrotactic microorganisms hybrid nanoliquid flow with the hall current and magnetic field over a spinning disk. *Sci. Reports* **2021**, *11*, 1−13.

(38) Nidhi; Kumar, L. Cu−Al2O3/engine oil Williamson hybrid nanofluid flow over a stretching/shrinking Riga plate with viscous dissipation and radiation effect. *Heat Transf* **2022**, *51*, 2279−2305.

(39) Gal, S.; et al. Three-Dimensional Study of Magneto-hydrodynamic NaturalConvection, Entropy Generation, and Electro-

https://doi.org/10.1021/acsomega.2c04600
ACS Omega 2022, 7, 36611−36622

magnetic Variables in aNanofluid Filled Enclosure Equipped with Inclined Fins. *ACS Omega* **2022**, *7*, 12365.
(40) Chu, Y. M.; Bashir, S.; Ramzan, M.; Malik, M. Y. Model-based comparative study of magnetohydrodynamics unsteady hybrid nanofluid flow between two infinite parallel plates with particle shape effects. *Math. Methods Appl. Sci.* **2022**, DOI: 10.1002/MMA.8234.
(41) Alshehri, A.; Shah, Z. Computational analysis of viscous dissipation and Darcy-Forchheimer porous medium on radioactive hybrid nanofluid. *Case Stud. Therm. Eng.* **2022**, *30*, 101728.
(42) Gamachu, D.; Ibrahim, W. Entropy production on couple-stress hybrid nanofluid flow in a rocket engine nozzle with non-Fourier's and non-Fick's law. *Ain Shams Eng. J.* **2022**, 101818.
(43) Alsaedi, A.; Muhammad, K.; Hayat, T. Numerical study of MHD hybrid nanofluid flow between two coaxial cylinders. *Alexandria Eng. J.* **2022**, *61*, 8355−8362.
(44) Bhatti, M. M.; Bég, O. A.; Abdelsalam, S. I. Computational Framework of Magnetized MgO−Ni/Water-Based Stagnation Nanoflow Past an Elastic Stretching Surface: Application in Solar Energy Coatings. *Nanomater* **2022**, *12*, 1049.
(45) Shahid, A.; Bhatti, M. M.; Ellahi, R.; Mekheimer, K. S. Numerical experiment to examine activation energy and bi-convection Carreau nanofluid flow on an upper paraboloid porous surface: Application in solar energy. *Sustain. Energy Technol. Assessments* **2022**, *52*, 102029.
(46) Bhatti, M. M.; et al. Lie group analysis and robust computational approach to examine mass transport process using Jeffrey fluid model. *Appl. Math. Comput.* **2022**, *421*, 126936.
(47) Sommerfield, C. M. Magnetic Dipole Moment of the Electron. *Phys. Rev.* **1957**, *107*, 328.
(48) Punith Gowda, R. J.; Naveen Kumar, R.; Prasannakumara, B. C.; Nagaraja, B.; Gireesha, B. J. Exploring magnetic dipole contribution on ferromagnetic nanofluid flow over a stretching sheet: An application of Stefan blowing. *J. Mol. Liq.* **2021**, *335*, 116215.
(49) Kumar, R. N.; et al. Impact of magnetic dipole on ferromagnetic hybrid nanofluid flow over a stretching cylinder. *Phys. Scr.* **2021**, *96*, 96.
(50) Gul, T.; et al. Magnetic Dipole Impact on the Hybrid Nanofluid Flow over an Extending Surface. *Sci. Reports* **2020**, *10*, 1−13.
(51) Shuaib, M.; Bilal, M.; Qaisar, S. Numerical study of hydrodynamic molecular nanoliquid flow with heat and mass transmission between two spinning parallel plates. *Phys. Scr.* **2020**, *96*, 025201.
(52) Shoaib, M.; et al. Soft computing paradigm for Ferrofluid by exponentially stretched surface in the presence of magnetic dipole and heat transfer. *Alexandria Eng. J.* **2022**, *61*, 1607−1623.
(53) Isa, F.; Zabiri, H.; Harun, N.; Shariff, A. M. CO2 Removal via an Environmental GreenSolvent, K2CO3−Glycine (PCGLY): InvestigativeAnalysis of a Dynamic and Control Study. *ACS Omega* **2022**, *7*, 18213.
(54) Hou, E.; et al.Dynamics of Tri-Hybrid Nanoparticles in the Rheology of Pseudo-Plastic Liquid with Dufour and Soret Effects. *Micromachines***2022**, *13*. DOI: 10.3390/mi13020201
(55) Muhammad, N.; Nadeem, S. Ferrite nanoparticles Ni-ZnFe2O4 , Mn- ZnFe2O4 and Fe2O4 in the flow of ferromagnetic nanofluid. *Eur. Phys. J. Plus* **2017**, *132*, 1−12.
(56) Nadeem, S.; Ahmad, S.; Muhammad, N. Analysis of ferrite nanoparticles in liquid. *Pramana* **2020**, *94*, 1−9.
(57) Gupta, S. K.; Modak, B.; Garcia, M. A. P.; Modak, P.; Mao, Y. Photon energy dependent appearance and disappearance of magnetic dipole transition in Gd2Hf2O7:Sm3+ nanophosphors. *J. Lumin.* **2022**, *245*, 118789.
(58) Mellado, P. Intrinsic topological magnons in arrays of magnetic dipoles. *Sci. Reports* **2022**, *121*, 1−15.
(59) Wang, F.; et al.*Numerical simulation of hybrid Casson nanofluid flow by the influence of magnetic dipole and gyrotactic microorganism*; Taylor & Francis, 2022.
(60) Zhang, H.-B.; Liu, C.-X.; Yang, J.-L.; Feng, T.-F.Muon anomalous magnetic dipole moment in the μ νSSM *. *Chinese Phys. C***2022**, *46*. DOI: 10.1088/1674-1137/AC71A6.
(61) Liao, S.*Homotopy analysis method in nonlinear differential equations*; Springer, 2012, pp 1−565.
(62) Liao, S.*Beyond perturbation : introduction to the homotopy analysis method*; Chapman & Hall/CRC, 2004.
(63) Liao, S. An optimal homotopy-analysis approach for strongly nonlinear differential equations. *Commun. Nonlinear Sci. Numer. Simul.* **2010**, *15*, 2003−2016.

https://doi.org/10.1021/acsomega.2c04600
ACS Omega 2022, 7, 36611−36622